

Photoionization of few electron systems with a hybrid Coupled Channels approach

Vinay Pramod Majety, Alejandro Zielinski and Armin Scrinzi[‡]

Physics Department, Ludwig Maximilians Universität, D-80333 Munich, Germany

Abstract. We present the hybrid anti-symmetrized coupled channels method for the calculation of fully differential photo-electron spectra of multi-electron atoms and small molecules interacting with strong laser fields. The method unites quantum chemical few-body electronic structure with strong-field dynamics by solving the time dependent Schrödinger equation in a fully anti-symmetrized basis composed of multi-electron states from quantum chemistry and a one-electron numerical basis. Photoelectron spectra are obtained via the time dependent surface flux (tSURFF) method. Performance and accuracy of the approach are demonstrated for spectra from the helium and beryllium atoms and the hydrogen molecule in linearly polarized laser fields at wavelength from 21 nm to 400 nm. At long wavelengths, helium and the hydrogen molecule at equilibrium inter-nuclear distance can be approximated as single channel systems whereas beryllium needs a multi-channel description.

Keywords: TDSE, Coupled Channels, Quantum Chemistry, tSURFF

[‡] Corresponding author: armin.scrinzi@lmu.de

1. Introduction

Understanding laser - atom/molecule interaction has become an important research pursuit with the introduction of many versatile light probes over the past decade. Promising experimental techniques like re-collision imaging [1] and attosecond streaking [2] are being pursued that aim to study time resolved electron dynamics. One of the factors that always creates a certain amount of vagueness in interpreting these strong field ionization experiments is the possible presence of multi-electron effects. An accurate interpretation of these experiments needs solutions of multi-electron time dependent Schrödinger equation (TDSE). As perturbation theory is not valid in strong field regime, one resorts to direct numerical solutions of the TDSE.

While simple single electron models or low dimensional models have been partially successful in explaining laser matter interactions, there have been several cases reported where a more elaborate description of electronic structure becomes important. Some of the examples include inter-channel coupling leading to an enhancement in high harmonic generation (HHG) from Xenon [3], modification of angle resolved ionization yield of CO_2 [4] and photoionization cross-sections in SF_6 [5], enhancement in HHG due to participation of doubly excited states in Beryllium [6], influence of nuclear motion [7], presence of conical intersections [8] and so on. All these instances need a more involved description of the electronic structure.

With one and two electron systems, a full dimensional numerical treatment is possible in linearly polarized laser fields. For systems with more than 6 degrees of freedom a full dimensional calculation is infeasible. There have been several efforts in the past decade to overcome this barrier of dimensionality for few electron systems by choosing only a part of the Hilbert space that is seemingly important for the dynamics. Some of the approaches that are being employed are time dependent configuration interaction methods [9], different variants of multi-configuration methods [10, 11, 12, 13], time dependent R-matrix method [14], and coupled channel methods [4].

One of the observables that is typically measured in strong laser - atom/molecule interaction experiments is photoelectron spectra. While the methods listed above [9, 10, 11, 12, 13, 14, 4] have tried to include multi-electron effects in photoionization studies, calculation of photoelectron spectra from multi-electron systems, especially at long wavelengths has remained out of computational reach. The particular difficulty arises from the fact that, in order to compute photoelectron spectra the asymptotic part of the wavefunction is required. This needs large simulation box volumes and access to exact single continuum states to project the wavefunction onto, at the end of time propagation. Having large simulation boxes and computing single continuum states of a multi-electron system are expensive tasks, making these kind of computations costly.

In this respect, a recently developed method called the time dependent Surface Flux (tSURFF) method [15, 16] has turned out to be an attractive solution. In the tSURFF approach, the wavefunction outside a certain simulation box is absorbed, and the electron flux through a surface before absorption is used to obtain photoelectron spectra. This way photoelectron spectra can be computed with minimal box sizes.

We aim to deal with the difficulties of the few body problem and computation of photoelectron spectra by combining quantum chemistry with tSURFF for single electron systems, through a coupled channels approach. Our coupled channels ansatz is similar in spirit to the one presented in [4]. However, unlike in [4], we deal with anti-symmetrization exactly. We discretize our multi-electron wavefunctions with the ground state of the system and anti-symmetrized products of the system's single ionic states and a numerical one-electron basis that we call the active electron basis. This ansatz is suitable to study single ionization problems. We compute the ionic and neutral states for our basis using the state of the art quantum chemistry code COLUMBUS [17] giving us the flexibility to treat the ionic states at various levels of quantum chemistry. While the fully flexible active electron basis describes the ionizing electron, the ionic basis describes the core polarization

and the exact anti-symmetrization ensures indistinguishability of the electrons. The inclusion of the field-free neutral helps us to get the right ionization potential and start with the correct initial state correlation without much effort. We call our method hybrid fully anti-symmetrized coupled channels method and use the acronym haCC to refer to it in this work. Using tSURFF with haCC, we compute photoelectron spectra with minimal box sizes.

We intend to communicate in this article the mathematical formulation of our method, and demonstrate its usefulness by computing photoelectron spectra of He , H_2 and Be in linearly polarized 21-400 nm wavelength laser fields and compare them with fully numerical two electron results. We discuss the advantages and limitations of such an approach through suitable examples.

2. Mathematical formulation

In this section, we describe our mathematical setup to solve the N-electron TDSE in the presence of an external laser field. We solve the TDSE

$$i\frac{\partial}{\partial t}\Psi = \hat{H}\Psi \quad (1)$$

with fixed nuclei approximation and with dipole approximation which implies neglecting the spatial dependence of the laser field. Atomic units are used unless specified otherwise. The non-relativistic N-electron field-free Hamiltonian can be written as:

$$\hat{H} = \sum_i \left[-\frac{1}{2}\nabla_i^2 - \sum_p \frac{Z_p}{|\vec{r}_i - \vec{a}_p|} \right] + \sum_{ij;i < j} \frac{1}{|\vec{r}_i - \vec{r}_j|} \quad (2)$$

where Z_p is the nuclear charge and \vec{a}_p are the nuclear coordinates of the p^{th} nuclei. The interaction with the external laser field in length gauge is given by:

$$\hat{D}_L = - \sum_j \vec{E}(t) \cdot \vec{r}_j \quad (3)$$

and in velocity gauge by

$$\hat{D}_V = \sum_j i\vec{A}(t) \cdot \vec{\nabla}_j. \quad (4)$$

We describe our multi-electron discretization in detail in 2.1, present the time propagation equations in 2.2 and the matrix elements in 2.3. The inverse of the overlap matrix can be computed efficiently using low rank updates which will be presented in 2.4. Treating anti-symmetrization exactly and including neutrals in our basis, introduces a technical difficulty in the form of linear dependencies in our basis. This is handled by performing a generalized inverse of the overlap matrix which will be presented in 2.5. We work in mixed gauge for the reasons detailed in [18] and briefed in 2.6. Finally, we present tSURFF for our coupled channels setup in section 2.7.

2.1. Multi-electron discretization

We discretize our N-electron wavefunction with the quantum chemistry ground state neutral wavefunction and anti-symmetrized products of an ionic basis and a numerical one-electron basis.

$$|\Psi(t)\rangle \approx \sum_{\mathcal{I}} |\mathcal{I}\rangle C_{\mathcal{I}}(t) + |\mathcal{G}\rangle C_{\mathcal{G}}(t) \quad (5)$$

where

$$|\mathcal{I}\rangle = \mathcal{A}[|i\rangle|I\rangle]. \quad (6)$$

Here, \mathcal{A} indicates anti-symmetrization, $|i\rangle$ are functions from a numerical one-electron basis that we call the active electron basis, $|I\rangle$ and $|\mathcal{G}\rangle$ are (N-1) and N particle functions respectively and $C_{\mathcal{I}}(t)$, $C_{\mathcal{G}}(t)$ are the time dependent coefficients.

The active electron is represented using finite elements for the radial coordinate and real spherical harmonics for the angular coordinates.

$$|i(\vec{r})\rangle = |f_i(r)\rangle |Y_{l_i m_i}(\Omega)\rangle \quad (7)$$

On each finite element we use high order scaled Legendre polynomials as basis functions. The typical orders we use are 10-14. The details of the finite element approach used here can be found in [19, 20]. A brief description is given in [Appendix A](#) for the convenience of the reader.

We choose $|I\rangle$ to be the eigenstates of the single ionic Hamiltonian obtained from the Multi-Reference Configuration Interaction Singles Doubles (MR-CISD) level of quantum chemistry. $|\mathcal{G}\rangle$ is chosen as the ground state of the system, also obtained from the MR-CISD level of quantum chemistry. These quantum chemistry wavefunctions are constructed with an atom centered primitive gaussian basis as the starting point. While $|\mathcal{G}\rangle$ is the lowest eigenvector of the N particle Hamiltonian with quantum chemistry, it is not the ground state of the Hamiltonian in our basis. Treating one of the electrons with the active electron basis that is superior to the gaussian basis improves the ground state.

The wavefunctions $|\mathcal{G}\rangle$ and $|I\rangle$ can be represented in a general form as sums of determinants:

$$|I\rangle = \sum_{p_1, p_2, \dots, p_{n-1}} d_{p_1, p_2, \dots, p_{n-1}} |\mathcal{A}[\phi_{p_1} \phi_{p_2} \dots \phi_{p_{n-1}}]\rangle \quad (8)$$

$$|\mathcal{G}\rangle = \sum_{p_1, p_2, \dots, p_n} d_{p_1, p_2, \dots, p_n} |\mathcal{A}[\phi_{p_1} \phi_{p_2} \dots \phi_{p_n}]\rangle \quad (9)$$

where ϕ_k are the Hartree-Fock orbitals of the neutral system. The same set of Hartree-Fock orbitals are used to construct both ionic and neutral CI functions. This allows us to use simple Slater-Condon rules to compute any matrix elements between them.

The explicit inclusion of the neutral ground state is motivated by the fact that, while the ionization process itself may be well described by one or few ionic channels, the initial ground state may be correlated. In order to avoid inclusion of many ionic states just to describe the initial state, we include the neutral ground state explicitly, thereby reducing the number of basis functions needed. This idea can be easily extended to include any specific correlated state that is of importance to a particular process. This gives the basis a capability to be engineered based on any existing knowledge of the ionization process. In the current work, we only include the neutral ground state in our basis.

2.2. Time propagation equations

Substituting our ansatz (5) into the TDSE (1) yields a set of coupled ordinary differential equations for the time dependent coefficients:

$$i \left[\langle \mathcal{G} | \mathcal{G} \rangle \frac{dC_{\mathcal{G}}}{dt} + \langle \mathcal{G} | \mathcal{I} \rangle \frac{dC_{\mathcal{I}}}{dt} \right] = \langle \mathcal{G} | \hat{H} | \mathcal{G} \rangle C_{\mathcal{G}} + \langle \mathcal{G} | \hat{H} | \mathcal{I} \rangle C_{\mathcal{I}} \quad (10)$$

$$i \left[\langle \mathcal{I} | \mathcal{G} \rangle \frac{dC_{\mathcal{G}}}{dt} + \langle \mathcal{I} | \mathcal{I} \rangle \frac{dC_{\mathcal{I}}}{dt} \right] = \langle \mathcal{I} | \hat{H} | \mathcal{G} \rangle C_{\mathcal{G}} + \langle \mathcal{I} | \hat{H} | \mathcal{I} \rangle C_{\mathcal{I}} \quad (11)$$

We time propagate the coefficients using an explicit fourth order Runge-Kutta method with an adaptive step size controller. In order to absorb the wavefunction at the box boundaries we use infinite range Exterior Complex Scaling (irECS) [19]. We typically choose simulation boxes larger than the

spatial extent of the Hartree-Fock orbitals and start absorption after the Hartree-Fock orbitals vanish. This implies that it suffices to complex scale only one of the N coordinates.

The cost of time propagation scales with the number of ionic states (say n_I) as n_I^2 and it is independent of the exact number of electrons. This makes basis sets of kind (5) attractive for treating many electron systems.

2.3. Matrix Elements

In order to solve the TDSE, we need to evaluate various operators in our chosen basis. Firstly, we introduce several generalized reduced density matrices that we need, with the help of creation (a_k^\dagger) and annihilation (a_k) operators on the single particle state ϕ_k . A p -th order generalized reduced density matrix between the $(N-1)$ particle ionic functions is given by:

$$\rho_{k_1, \dots, k_p, l_1, \dots, l_p}^{IJ} = \langle I | a_{k_1}^\dagger \dots a_{k_p}^\dagger a_{l_1} \dots a_{l_p} | J \rangle \quad (12)$$

Similarly, we define generalized Dyson coefficients between the N -particle neutral wavefunctions and $(N-1)$ particle ionic wavefunctions as

$$\eta_{k_1, \dots, k_p, l_1, \dots, l_{p-1}}^{\mathcal{G}J} = \langle \mathcal{G} | a_{k_1}^\dagger \dots a_{k_p}^\dagger a_{l_1} \dots a_{l_{p-1}} | J \rangle \quad (13)$$

With the help of these objects, we present below the final form of the matrix elements. The overlap matrix has the form

$$\begin{aligned} \langle \mathcal{G} | \mathcal{G} \rangle &= 1 \\ \langle \mathcal{G} | \mathcal{I} \rangle &= \eta_k^{\mathcal{G}I} \langle \phi_k | i \rangle \\ \langle \mathcal{I} | \mathcal{J} \rangle &= \langle i | j \rangle \langle I | J \rangle - \langle i | \phi_l \rangle \rho_{kl}^{IJ} \langle \phi_k | j \rangle \\ &= \langle i | j \rangle \delta_{IJ} - \langle i | \phi_l \rangle \rho_{kl}^{IJ} \langle \phi_k | j \rangle \end{aligned} \quad (14)$$

where $\eta_k^{\mathcal{G}I}$ can be identified with the Dyson orbital coefficients with respect to the Hartree-Fock orbitals and ρ_{kl}^{IJ} are the one particle reduced density matrices.

The single particle operators have the form:

$$\hat{T} = \hat{t}(1) + \hat{t}(2) + \dots + \hat{t}(N) \quad (15)$$

where $\hat{t}(u)$ is the single particle operator corresponding to the coordinate u . The matrix elements with respect to the basis (5) take the form:

$$\begin{aligned} \langle \mathcal{G} | \hat{T} | \mathcal{G} \rangle &= \rho_{kl}^{\mathcal{G}\mathcal{G}} \langle \phi_k | \hat{t} | \phi_l \rangle \\ \langle \mathcal{G} | \hat{T} | \mathcal{I} \rangle &= \eta_k^{\mathcal{G}I} \langle \phi_k | \hat{t} | i \rangle + \eta_{klm}^{\mathcal{G}I} \langle \phi_k | \hat{t} | \phi_m \rangle \langle \phi_l | i \rangle \\ \langle \mathcal{I} | \hat{T} | \mathcal{J} \rangle &= \langle i | j \rangle \langle I | \hat{t} | J \rangle + \langle i | \hat{t} | j \rangle \langle I | J \rangle - \langle i | \hat{t} | \phi_l \rangle \rho_{kl}^{IJ} \langle \phi_k | j \rangle \\ &\quad - \langle i | \phi_l \rangle \rho_{kl}^{IJ} \langle \phi_k | \hat{t} | j \rangle - \langle i | \phi_c \rangle \langle \phi_a | j \rangle \langle \phi_b | \hat{t} | \phi_d \rangle \rho_{abcd}^{IJ} \end{aligned} \quad (16)$$

where $\eta_{klm}^{\mathcal{G}I}$ are the three index generalized Dyson coefficients, Eq.(13), and ρ_{abcd}^{IJ} are the two particle reduced density matrices, Eq. (12).

Finally, the two particle operators have the form:

$$\hat{V}^{(2)} = \sum_{ij; i < j} \hat{v}(ij) \quad (17)$$

with the matrix elements

$$\begin{aligned}
\langle \mathcal{G} | \hat{V}^{(2)} | \mathcal{G} \rangle &= \frac{1}{2} \rho_{abcd}^{\mathcal{G}\mathcal{G}} \langle \phi_a \phi_b | \hat{v} | \phi_c \phi_d \rangle \\
\langle \mathcal{G} | \hat{V}^{(2)} | \mathcal{I} \rangle &= \eta_{klm}^{\mathcal{G}I} \langle \phi_k \phi_l | \hat{v} | \phi_m i \rangle + \frac{1}{2} \eta_{abcde}^{\mathcal{G}I} \langle \phi_a \phi_b | \hat{v} | \phi_d \phi_e \rangle \langle \phi_c | i \rangle \\
\langle \mathcal{I} | \hat{V}^{(2)} | \mathcal{J} \rangle &= \frac{1}{2} \rho_{abcd}^{\mathcal{I}\mathcal{J}} \langle \phi_a \phi_b | \hat{v} | \phi_c \phi_d \rangle \langle i | j \rangle + \underbrace{\rho_{kl}^{IJ} \langle \phi_k i | \hat{v} | \phi_l j \rangle}_{\text{Direct term}} - \underbrace{\rho_{kl}^{IJ} \langle \phi_k i | \hat{v} | j \phi_l \rangle}_{\text{Standard exchange term}} \\
&\quad - \underbrace{\rho_{abcd}^{IJ} \langle \phi_a i | \hat{v} | \phi_c \phi_d \rangle \langle \phi_b | j \rangle - \rho_{abcd}^{IJ} \langle \phi_a \phi_b | \hat{v} | \phi_c j \rangle \langle i | \phi_d \rangle - \frac{1}{2} \rho_{abcdef}^{IJ} \langle \phi_a \phi_b | \hat{v} | \phi_d \phi_e \rangle \langle i | \phi_f \rangle \langle \phi_c | j \rangle}_{\text{Other exchange terms due to non-orthogonality}}
\end{aligned} \tag{18}$$

where $\eta_{abcde}^{\mathcal{G}I}$ are the five index generalized Dyson coefficients, Eq.(13) and ρ_{abcdef}^{IJ} are the three particle reduced density matrices, Eq. (12).

In order to compute the two-electron integrals, we first project the Hartree-Fock orbitals onto a single center expansion:

$$\phi_k(\vec{r}) = \sum_{q_k l_k m_k} d_{q_k l_k m_k} Y_{l_k m_k}(\theta, \phi) \tag{19}$$

where q_k are some radial quadrature points, l_k, m_k refer to the angular momentum functions and use these expansions with the multi-pole expansion:

$$\frac{1}{|\vec{r}_1 - \vec{r}_2|} = \sum_{LM} \frac{4\pi}{2L+1} \frac{r_{<}^L}{r_{>}^{L+1}} Y_{LM}(\theta_1, \phi_1) Y_{LM}^*(\theta_2, \phi_2) \tag{20}$$

with $r_{<} = \min(r_1, r_2)$ and $r_{>} = \max(r_1, r_2)$. These two particle operators pose a challenge for efficient computation. While the direct term is relatively easy to handle, the exchange terms consume a major portion of the Hamiltonian setup time.

2.4. Inverse of the overlap matrix

The overlap matrix (14) does not have the form of an overlap of a standard finite element basis. The overlap of a standard finite element basis has a banded structure that usually helps in an efficient computation of the inverse. Non-orthogonality between the active electron basis and the Hartree-Fock orbitals leads to extra cross terms that destroy the banded structure in general and complicate the computation of the inverse. However, the inverse of the overlap can still be computed efficiently using low rank updates. We use here the Woodbury formula [21] to compute our inverse, according to which, the inverse of a modified matrix of the form $(S_0 - U\Lambda U^\dagger)$ can be computed as:

$$\begin{aligned}
S^{-1} &= (S_0 - U\Lambda U^\dagger)^{-1} \\
&= S_0^{-1} - S_0^{-1} U (U^\dagger S_0^{-1} U - \Lambda^{-1})^{-1} U^\dagger S_0^{-1}
\end{aligned} \tag{21}$$

As an example with 2 ionic states and 1 neutral, we show that the overlap matrix (14) can be cast in the form:

$$S = \underbrace{\begin{pmatrix} s_0 & 0 & 0 \\ 0 & s_0 & 0 \\ 0 & 0 & 1 \end{pmatrix}}_{S_0} - \underbrace{\begin{pmatrix} u & 0 & 0 \\ 0 & u & 0 \\ 0 & 0 & 1 \end{pmatrix}}_U \underbrace{\begin{pmatrix} \rho^{11} & \rho^{12} & \eta^{\mathcal{G}1} \\ \rho^{21} & \rho^{22} & \eta^{\mathcal{G}2} \\ [\eta^{\mathcal{G}1}]^T & [\eta^{\mathcal{G}2}]^T & 0 \end{pmatrix}}_\Lambda U^\dagger \tag{22}$$

which resembles the left hand side of the Woodbury formula (21). Here, $(s_0)_{ij} = \langle i | j \rangle$ and $u_{ik} = \langle i | \phi_k \rangle$. If n_i is the number of active electron basis functions and n_{hf} be the number of Hartree-Fock orbitals

that is much smaller than n_i , then the dimensions of s_0 are $n_i \times n_i$ and the dimensions of matrix u are $n_i \times n_{hf}$.

Let n_I be the number of ionic states in general. Then the dimensions of the overlap matrix S and S_0 are $(n_I n_i + 1) \times (n_I n_i + 1)$. The dimensions of the matrix U are $(n_I n_i + 1) \times (n_I n_{hf} + 1)$ and the matrix Λ are $(n_I n_{hf} + 1) \times (n_I n_{hf} + 1)$. This low rank structure of the extra correction terms can be utilized to compute the inverse efficiently by using the Woodbury formula.

2.5. Handling linear dependencies

Anti-symmetrization and non-orthogonality of the active electron basis with respect to the Hartree-Fock orbitals may render our basis linearly dependent. If the $\{|i\rangle\}$ -basis is near-complete w.r.t. the HF-orbital basis

$$\langle \phi_k | i \rangle [s_0^{-1}]_{ij} \langle j | \phi_l \rangle \approx \delta_{kl}, \quad (23)$$

it is possible to find coefficients $c_{i,I}$ such that

$$\sum_{i,I} c_{i,I} \mathcal{A}[|i\rangle|I\rangle] \approx 0. \quad (24)$$

A simple case when this can happen is, if one and the same HF orbital appears in all the ionic determinants, which renders all neutral determinants involving the complete basis = 0. This makes the overlap matrix non-invertible. A possible solution would be to orthogonalize the active electron basis with respect to the Hartree-Fock orbitals. But this is not an easily implementable solution with a CI ionic basis. For each determinant, the set of Hartree-Fock orbitals with respect to which the active electron basis must be orthogonal is different.

As an alternative solution we use a generalization of the Woodbury formula (21) to compute the inverse of a matrix only on the subspace of the non-zero eigenvectors of the matrix. Let D denote the $n_0 \times n_z$ matrix of eigenvectors with near-zero eigenvalues $z_p < \epsilon, p = 1, \dots, n_z$ of the generalized eigenvalue problem

$$SD = S_0 D z, \quad (25)$$

with z denoting diagonal matrix of the eigenvalues z_p and D satisfying the orthonormality relation $D^\dagger S_0 D = \mathbf{1}$. In general, there will be comparatively few such eigenvectors $n_z \ll n_0$ that can be easily determined by an iterative solver. We can remove these singular vectors from our calculation by the projector

$$Q = 1 - DD^\dagger S_0. \quad (26)$$

The projector property $Q^2 = Q$ can be easily verified. As the projector refers to the generalized eigenvalue problem with $S_0 \neq \mathbf{1}$, Q is not an orthogonal projector, that is $Q^\dagger \neq Q$. We define a pseudo-inverse \tilde{S}^{-1} of the restricted S on the subspace of generalized eigenvectors with non-zero eigenvalues with the property

$$\tilde{S}^{-1} S Q = Q. \quad (27)$$

One can verify directly that the generalized Woodbury formula

$$\tilde{S}^{-1} = Q S_0^{-1} [1 - U(U^\dagger Q S_0^{-1} U - \Lambda)^{-1} U^\dagger Q S_0^{-1}] \quad (28)$$

satisfies the definition (27). The matrix $(U^\dagger Q S_0^{-1} U - \Lambda)$ is invertible on all vectors appearing in $U^\dagger Q$ to its right, as exactly the singular vectors are removed by the projector Q . Apart from the necessity to determine D during setup, the correction does not significantly increase the operations count for the inverse overlap.

2.6. Choice of gauge

In [18], we had shown that when an electron is treated with a restricted basis, for example, in terms of a few bound states, the length gauge is a more natural gauge. Compared to pure velocity gauge, the coupled channel computations converge quickly in mixed gauge with length gauge spanning the region of the ionic states and velocity gauge thereafter for asymptotics. In this current work, we use continuous gauge switching, detailed in [18], for its easy implementation. We use the resulting TDSE after the length gauge form is transformed using the following transformation.

$$U_c = \begin{cases} 1 & \text{for } r \leq r_g \\ \exp \left[i \vec{A}(t) \cdot \sum_{j=1}^N \hat{r}_j (r_j - r_g) \right] & \text{for } r > r_g \end{cases} \quad (29)$$

Here, r_g is the gauge radius that separates the length gauge and velocity gauge regions.

2.7. Computation of photoelectron spectra

Computation of photoelectron spectra is expensive for two reasons. (1) The asymptotic part of the wavefunction is needed to extract photoelectron spectra, which means large simulation boxes to preserve the asymptotic part and to avoid any numerical reflections that may corrupt the wavefunction. (2) Single continuum states are needed into which the wavefunction must be decomposed, in order to obtain photoelectron spectra. These two problems are circumvented in a recently developed method tSURFF[15, 16] by computing photoelectron spectra, through a time integration of electron flux flowing through a surface defined by a radius R_c called the tSURFF radius. The Coulomb potential is smoothly turned off before R_c , which implies that the scattering solutions thereafter are well known Volkov solutions. R_c becomes a convergence parameter, and by varying this radius, one can compute spectra to a given accuracy. This method has been explained in detail in previous works for single ionization in [15] and for double ionization in [16]. A proposal for extension of this method for single ionization of multi-electron systems has been outlined in [15]. We describe here the application of the method with our coupled channels setup.

Let χ_k be the scattering solutions which take the form of Volkov solutions beyond R_c and $\Psi(T)$ be the wavefunction at some large time T . According to tSURFF for single electron systems, photoelectron spectra can be computed as $\sigma_k = |b_k|^2$ with b_k defined as:

$$\begin{aligned} b_k &= \langle \chi_k(T) | \Theta(R_c) | \Psi(T) \rangle \\ &= i \int_0^T dt \langle \chi_k(t) | \left[-\frac{1}{2} \Delta + i \vec{A}(t) \cdot \vec{\nabla}, \Theta(R_c) \right] | \Psi(t) \rangle \end{aligned} \quad (30)$$

Here $\Theta(R_c)$ is a Heaviside function that is unity for $r > R_c$ and 0 elsewhere.

This formulation can be easily extended to the N electron problem in a coupled channels setup. In this setup, we mostly take a set of ionic bound states for the ionic basis. These states have a finite extent. We may choose R_c such that the electrons described by the ionic basis vanish by R_c which means all the exchange terms in the Hamiltonian vanish after R_c . The remaining direct potential can be smoothly turned off just as the Coulomb potential. This implies that the wavefunction beyond R_c evolves by the Hamiltonian:

$$H(r > R_c) = H_{ion} \otimes \hat{1} + \hat{1}_{ion} \otimes \left[-\frac{1}{2} \Delta + i \vec{A}(t) \cdot \vec{\nabla} \right] \quad (31)$$

that allows for a complete set of solutions of the form:

$$\xi_{c,k}(\vec{r}_1, \dots, \vec{r}_n, t) = \mathcal{A} [\kappa_c(\vec{r}_1, \dots, \vec{r}_{n-1}, t) \otimes \chi_k(\vec{r}_n, t)] \quad (32)$$

where H_{ion} is the single ionic Hamiltonian and $\kappa_c(t)$ are time dependent ionic channel functions solving the TDSE

$$i\frac{\partial\kappa_c(t)}{\partial t} = \hat{H}_{ion}\kappa_c(t) \quad (33)$$

within the ansatz in terms of field-free ionic states

$$|\kappa_c(t)\rangle = \sum_I |I\rangle d_{cI}(t). \quad (34)$$

With the help of the $\xi_{c,k}$, channel resolved photoelectron spectra can be computed as

$$\sigma_{c,k} = |\langle \xi_{c,k}(\vec{r}_1, \dots, \vec{r}_n, T) | \Theta(R_c) | \Psi(\vec{r}_1, \dots, \vec{r}_n, T) \rangle|^2 \quad (35)$$

and the asymptotic decomposition of Ψ in terms of $\xi_{c,k}$ is obtained as

$$\begin{aligned} & \langle \xi_{c,k}(\vec{r}_1, \dots, \vec{r}_n, T) | \Theta(R_c) | \Psi(\vec{r}_1, \dots, \vec{r}_n, T) \rangle \\ &= i \int_0^T dt \langle \mathcal{A}[\kappa_c(\vec{r}_1, \dots, \vec{r}_{n-1}, t) \otimes \chi_k(\vec{r}_n, t)] \left[-\frac{1}{2}\Delta_n + i\vec{A}(t) \cdot \vec{\nabla}_n, \Theta_n(R_c) \right] | \Psi(\vec{r}_1, \dots, \vec{r}_n, t) \rangle \\ &= i \int_0^T dt \langle \chi_k(\vec{r}_n, t) \left[-\frac{1}{2}\Delta_n + i\vec{A}(t) \cdot \vec{\nabla}_n, \Theta_n(R_c) \right] | \zeta_c(\vec{r}_n, t) \rangle \end{aligned} \quad (36)$$

where

$$\zeta_c(\vec{r}_n, t) = \langle \kappa_c(\vec{r}_1, \dots, \vec{r}_{n-1}, t) | \Psi(\vec{r}_1, \dots, \vec{r}_n, t) \rangle \quad (37)$$

are Dyson-like orbitals. The commutator of the derivatives with the Heaviside function Θ gives δ -like terms involving values and derivatives of Ψ at the surface $|\vec{r}| = R_c$. As we choose R_c such that the Hartree-Fock orbitals vanish by then, we don't need to consider the exchange terms in computing ζ_c . Along with time propagating the N electron problem, one needs to also time propagate the ionic problem (33).

2.8. Spin symmetry

As we solve the non-relativistic TDSE, the total spin of the system is conserved during the time evolution. We can therefore remove the spin degree of freedom through suitable linear combinations of the anti-symmetrized products in the basis (5) to enforce a particular spin symmetry. This reduces the size of our basis. We consider only singlet spin symmetric systems in this work. As an example, we show how singlet spin symmetry can be enforced. Let \uparrow and \downarrow indicate the spin states $\pm\frac{1}{2}$ associated with a spatial function. Choosing linear combinations of the kind:

$$\mathcal{A}[|I\rangle|i\rangle] := \frac{\mathcal{A}[|I^\uparrow\rangle|i^\downarrow\rangle] - \mathcal{A}[|I^\downarrow\rangle|i^\uparrow\rangle]}{\sqrt{2}} \quad (38)$$

enforces singlet symmetry. This can be extended to creating linear combinations that enforce an arbitrary spin symmetry.

3. Two-electron benchmark calculations

We use two-electron full dimensional calculations (full-2e) as benchmark for our haCC computations. We solve the two-electron TDSE using an independent particle basis of the form:

$$\Psi(\vec{r}_1, \vec{r}_2, t) = \sum_{k_1 k_2 l_1 l_2 m} c_{k_1 k_2 l_1 l_2 m}(t) f_{k_1}(r_1) f_{k_2}(r_2) Y_{l_1 m}(\theta_1, \phi_1) Y_{l_2 -m}(\theta_2, \phi_2) \quad (39)$$

where $c_{k_1 k_2 l_1 l_2 m}(t)$ are the time dependent coefficients, $f_{k_1}(r_1), f_{k_2}(r_2)$ are functions from a finite element discretization of the same type as for our active electron basis and Y_{lm} are spherical harmonics. We use the same type of single center expansion for all the benchmark computations. A complete description of this method will be presented elsewhere [20]. Solving the TDSE with the expansion (39) needs much larger computational resources compared to the haCC approach.

4. Single photoelectron spectra

In this section, we present photoelectron spectra from helium and beryllium atoms and from the hydrogen molecule with linearly polarized laser fields computed with the above described coupled channels formalism. We also present the single photon ionization cross-sections for the beryllium atom and wavelength dependence of ionization yield for the hydrogen molecule to compare with other existing calculations. We use \cos^2 envelope pulses for all the calculations and the exact pulse shape is given as

$$A_z(t) = A_0 \cos^2\left(\frac{\pi t}{2cT}\right) \sin\left(\frac{2\pi t}{T} + \beta\right) \quad (40)$$

$$E_z(t) = -\frac{dA_z(t)}{dt} \quad (41)$$

where A_0 is the peak vector potential, T is the single cycle duration, c is the number of laser cycles and β is the carrier envelope phase. We compare our results for helium and the hydrogen molecule with full-2e calculations [20] and for beryllium with effective two electron model calculations.

The convergence of the benchmark calculations and the haCC calculations were done systematically and independently. All the spectra presented here were computed with simulation box sizes on the scale of 30-50 a.u. The radial finite element basis consisted of high order polynomials typically of orders 10-14 and the total number of radial basis functions was such that there were 2-3 functions per atomic unit. The angular momenta requirement strongly depends on the wavelength. The longer wavelengths needed larger number of angular momenta for convergence.

4.1. Helium

Helium is the largest atom that can be numerically treated in full dimensionality. With linearly polarized laser fields, the symmetry of the system can be used to reduce the problem to 5 dimensions. The energies of helium ionic states are $-2n^{-2}$ for principal quantum number n . The first two ionic states are separated by 1.5 a.u in energy, which is large, for example, compared to a photon energy of 0.456 a.u at 100nm. This has been a motivation to treat helium as an effective single electron system with XUV and longer wavelengths in some earlier works, for example in [22]. We examine below, the validity of treating helium as an effective single electron system, by comparing haCC calculations with full dimensional calculations at different wavelengths.

Figure 1 shows photoelectron spectra from helium with a 21 nm ($\omega = 2.174$ a.u), 3 cycle laser pulse with a peak intensity of $10^{15} \text{W}/\text{cm}^2$. The one and two photon ionization peaks of $1s$ and $2p_z$ channel spectra are shown. The relative errors of haCC calculations are computed with respect to the full dimensional calculation. The single photon peak of the $1s$ channel is computed to a few percent accuracy, except for a feature around 1.3 a.u., with a single ionic state. The resonant feature can be identified with the $2s2p$ doubly excited state [23], which is reproduced to few percent accuracy with the addition of 2nd shell ionic states. While the position of the resonance is reproduced accurately in the calculations presented here, the propagation time was well below the life-time of this resonance which is reflected in the width of the feature that is well above the natural line width. It should be emphasized that the exact width emerges when propagation times are extended to large times comparable to the decay times of the doubly excited state. The two photon peak of the $1s$ channel

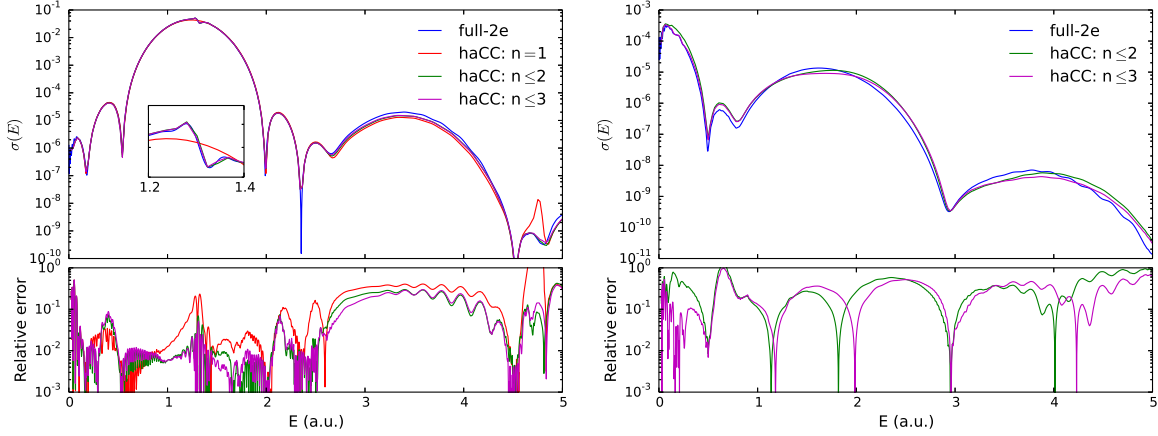


Figure 1. Photoelectron spectra from helium with 3-cycle, 21nm laser pulse with a peak intensity of $10^{15} W/cm^2$. Left figure: ground state channel ($1s$), Right figure: a first excited state channel ($2p_z$). The upper panels show spectra obtained with a full-2e and haCC calculations with different number of ionic states included as indicated in the legend. Here, n is the principal quantum number. The lower panels show relative errors of haCC calculations with respect to full-2e calculations. The inset shows the $2s2p$ resonance (see main text).

and the $2p_z$ channel spectra need more than a single ionic state and they could be computed only up to 15% accuracy even after inclusion of 9 ionic states ($n \leq 3$).

A broadband (few cycle) XUV pulse tends to excite the initial state into a band of final states which may include many correlated intermediate states. Here, the intrinsic limitations of any coupled channels approach that is based on ionic bound states only are exposed. Firstly, a correlated intermediate state with a bound character needs large number of ionic states to be correctly represented. Secondly, the ionic bound states based on gaussian basis sets do not have the exact asymptotic behavior. This can lead to an inaccuracy in length gauge dipole matrix elements. Finally, the absence of ionic continuum states in our approach can lead to another source of inaccuracy. Due to these limitations, we do not expect the shake-up channel spectra to be more accurate than 10-15%.

Figure 2 shows total photoelectron spectra from helium at 200nm and 400nm wavelengths. The exact laser parameters are indicated in the figure captions. At 200nm ($\omega = 0.228a.u.$), the ionization threshold is four photons. A single ionic state calculation produces spectra that are 10% accurate with respect to a full dimensional calculation. Addition of second and third shell ionic states improves the accuracy of the spectra to few percent level in the important regions of the spectrum. At 400nm ($\omega = 0.114a.u.$), the ionization threshold is 8 photons. Also here, a single ionic state computation produces spectra that are 10% accurate with respect to a full dimensional calculation. Addition of more ionic states, does not improve the accuracy further. This is possibly due to the missing continuum of the second electron that is needed to fully describe the polarization of the ionic core.

At longer wavelengths, we find that single ionic state computations are sufficient to produce spectra accurate on the level of 10%. This is consistent with the knowledge that at longer wavelengths, it is the ionization thresholds that play a more important role in determining the ionization yields compared to the exact electronic structure. Our findings show that helium at long wavelengths can be approximated as a single channel system.

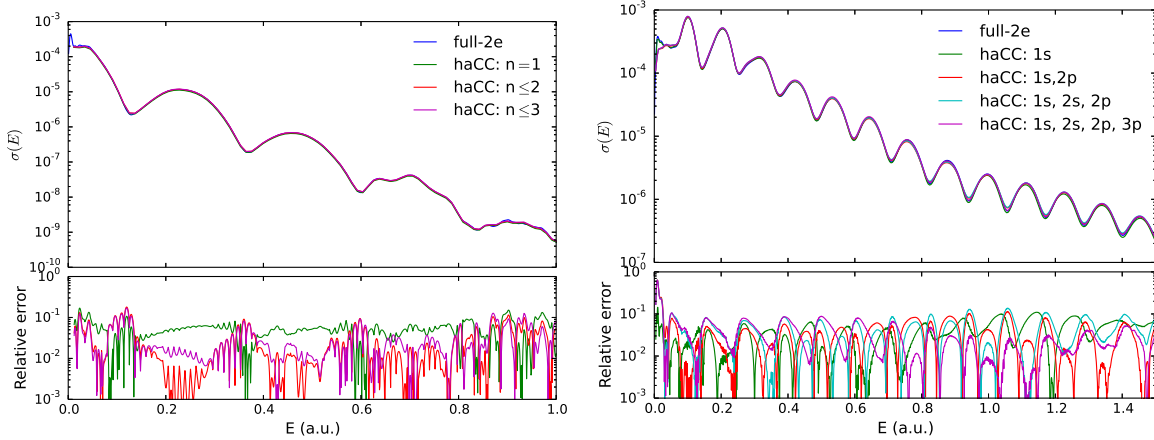


Figure 2. Total photoelectron spectra from helium with Left figure: 3-cycle, 200nm laser pulse with a peak intensity of $10^{14}W/cm^2$, Right figure: 3-cycle, 400nm laser pulse with a peak intensity of $3 \times 10^{14}W/cm^2$. The upper panels show spectra obtained with a full-2e and haCC calculations with different number of ionic states included as indicated in the legend. Here, n is the principal quantum number. The lower panels show relative errors of haCC calculations with respect to full-2e calculation

4.2. Beryllium

Beryllium is a four electron system that is often treated as a two electron system due to the strong binding of its inner two electrons. The third ionization potential of beryllium is 153.8961 eV [24]. With photon energies below this third ionization potential, it can be safely treated as an effective two electron system. This allows us to have a benchmark for our spectra by adapting the simple Coulomb potential to an effective potential in our two electron code. We use the effective potential given in [6] for our benchmark calculations. We refer to these as ‘effective-2e’ calculations.

Table 1 lists the energies of the first 8 ionic states of beryllium relative to the ground ionic state. Unlike in helium, the ionic states are closely spaced in energy and one would expect inter-channel couplings to play a greater role.

Ionic state	NIST database (eV)	Columbus energies (eV)
$1s^2 2s$	0.0	0.0
$1s^2 2p$	3.9586	3.9767
$1s^2 3s$	10.9393	10.9851
$1s^2 3p$	11.9638	12.1407

Table 1. Energies of the used single ionic states of Beryllium relative to the ground state ion. The COLUMBUS[17] ionic states are computed at MR-CISD level with aug-cc-pvtz basis.

Figure 3 shows photoelectron spectra from beryllium with 21nm and 200nm wavelength laser pulses. The exact parameters are indicated in the figure caption. The relative errors of spectra from the haCC calculations are computed with respect to the effective-2e calculations.

At 21nm, the one and two photon ionization peaks of ground state channel spectra are shown. Here, the single photon ionization process itself needs more than the ground ionic state to produce accurate photoelectron spectra. Adding more ionic states improves the accuracy to a few percent

level. We find that the close energetic spacing of beryllium ionic states, leads to a greater possibility of inter-channel coupling that is manifested in the form of the single ionization continuum needing more than the ground ionic state to be well represented.

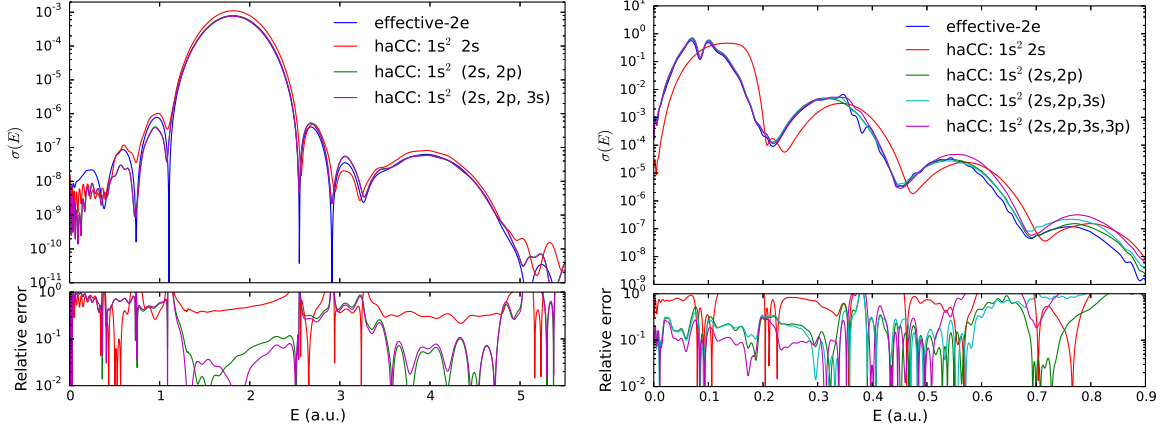


Figure 3. Photoelectron spectra from the beryllium atom. Left figure: Ground state channel spectra with 3-cycle, 21nm laser pulse with a peak intensity of $10^{15}W/cm^2$. Right figure: Total spectra with 3-cycle, 200nm laser pulse with a peak intensity of $10^{14}W/cm^2$. The upper panels show spectra obtained with effective-2e and haCC calculations with different number of ionic states included as indicated in the legend. The lower panels show relative errors of haCC calculations with respect to the effective-2e calculations.

Also at 200nm, we need more than the ground ionic state to compute realistic spectra. With $1s^22s$, $1s^22p$ ionic states included, the spectra produced have 20% accuracy with respect to the benchmark calculation. With the addition of $1s^23s$ and $1s^23p$ states, a structure similar to the one predicted by the benchmark calculation develops around 10 eV. This structure may be identified with the lowest resonance $1s^22p3s$ at 10.71 eV [6]. The coupled channels calculations with the number of ionic states considered here, however do not reproduce the structure on the second peak exactly. This points to a feature of a coupled channels basis that, the correct representation of a strongly correlated state that has bound character requires a large number of ionic states. As an alternative strategy, one can explicitly include the correlated state of importance into the basis, if it can be pre-computed, on the same footing as the correlated ground state.

It has been shown through examples in section 4.1 that helium can be modeled as single channel system at longer wavelengths. Lithium, the smallest alkali metal, also has been successfully modeled as a single electron system in an effective potential, for example in [25]. We find that beryllium needs at least two ionic states - $1s^22s$ and $1s^22p$ for a realistic modeling. It serves as a first simple example where single electron models break down and multiple channels need to be considered.

In figure 4, we present the single photon ionization cross-sections as a function of photon energy from our haCC method and compare them with the cross-sections calculated with TD-RASCI method [11] and R-matrix method [26] and with experimental results from [27]. The cross-sections in our time dependent approach are computed using the Eq (51) given in ref [14] with which the N photon ionization cross-section, $\sigma^{(N)}$ in units cm^{2N}/s^{N-1} can be computed as:

$$\sigma^{(N)} = (8\pi\alpha)^N \left(\frac{3.5 \times 10^{16}}{I} \right)^N \omega^N \Gamma a_0^{2N} t_0^{N-1} \quad (42)$$

where I is the intensity in W/cm^2 , ω is the laser frequency in a.u., α is the fine structure constant and

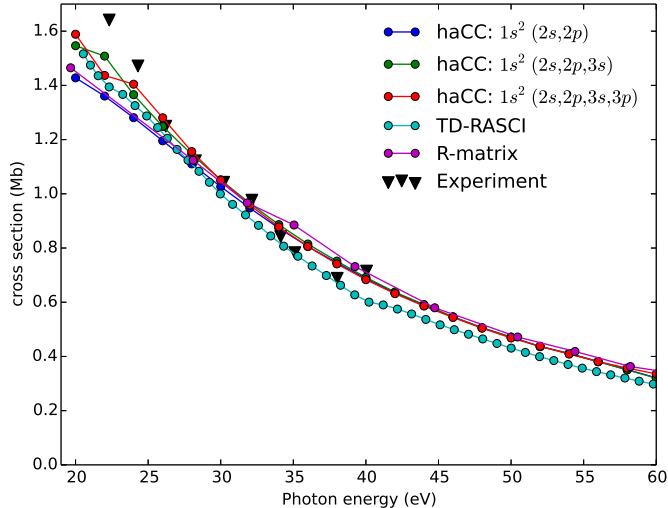


Figure 4. Single photoionization cross-sections for beryllium in the photon range of 20-60 eV. Presented are results from haCC calculations with 4,5,8 ionic states. The figure shows a comparison with earlier calculations using TD-RASCI method [11], R-matrix method [26] and with experimental results from [27]

a_0 , t_0 are atomic units of length and time respectively. Γ is the total ionization rate which is computed in a time dependent approach by monitoring the rate at which the norm of the wavefunction in a certain inner region drops. We use for our computations a 40-cycle continuous wave laser pulse with a 3 cycle \cos^2 ramp up and ramp down and with an intensity of $10^{12} \text{W}/\text{cm}^2$.

All the theoretical methods agree with each other qualitatively, though there are differences on the level of 5-10% quantitatively. The experimental results from [27] have error bars on the level $\lesssim 10\%$ (0.1 Mb) which are not shown here. All the theoretical results lie in this range except at low energies. In the higher photon energy range, 30-60 eV, the haCC results and the R-matrix results are in good agreement compared to the TD-RASCI. In the haCC calculations, including more than 4 ionic states does not change the cross-sections. In the photon energy range 20-30 eV, the haCC computations with 5 and 8 ionic states are in good agreement with TD-RASCI results compared to the R-matrix results. In this energy range, the cross-sections from haCC calculations show a dependence on the number of ionic states included. This modulation may be attributed to the presence of auto-ionizing states in this region. Table III in [6] presents a list of resonances that appear in beryllium electronic structure. The first ionization potential is 9.3 eV. With photon energies around 20 eV, the resulting photoelectron reaches continuum region where a number of resonances are present. As correlated resonances need many ionic states to be well represented in a coupled channels basis, this may explain the dependence of the cross-section on the number of ionic states in 20-30 eV photon range.

4.3. Hydrogen molecule

The hydrogen molecule in linearly polarized laser fields parallel to the molecular axis, with fixed nuclei has the same symmetry as helium in linearly polarized laser fields. The off-centered nuclear potential, however, increases the angular momenta requirement when treated with a single center expansion. While the number of required basis functions can be reduced through a choice of a more natural coordinate system like prolate spheroidal coordinates for diatomics [28], the challenge of computing two electron integrals remains. In the case of hydrogen molecule at equilibrium internuclear distance

($R_0 = 1.4$ a.u.), a calculation with single center expansion easily converges, as the light hydrogen nuclei do not significantly distort the spherical symmetry of the electron cloud. As a benchmark for spectra, we use results from a full dimensional calculation, that expands the wavefunction in a single center basis.

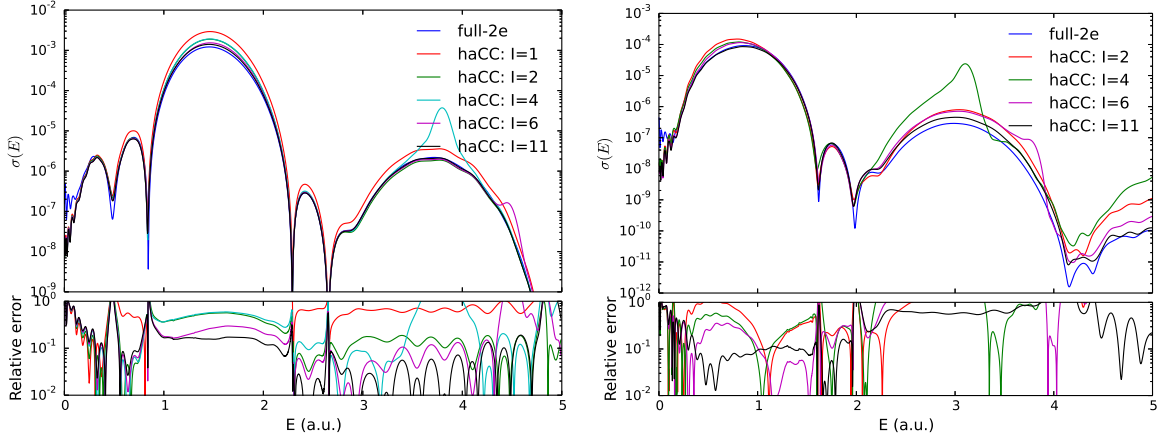


Figure 5. Photoelectron spectra from H_2 with a 3-cycle 21nm laser pulse with a peak intensity of $10^{15} W/cm^2$. Left figure: Ground state channel ($1\sigma_g$) Right figure: First excited state channel ($1\sigma_u$). The upper panels show spectra obtained with full-2e and haCC calculations with different number of ionic states (I) included (as indicated in the legend). The lower panels show relative errors of haCC calculations with respect to the full-2e calculation. With $I=4,6$, there are visible artefacts on the 2 photon peaks around 3 a.u. which are explained in the text.

Figure 5 shows photoelectron spectra from H_2 at 21nm wavelength. The exact laser parameters are given in the figure caption. The ground state ($1\sigma_g$) and first excited state ($1\sigma_u$) channel spectra are shown. We find that, at this wavelength, a single ionic state is not sufficient to produce accurate photoelectron spectra. With the addition of more ionic states, there is a systematic improvement in the accuracy of the calculations. With 11 lowest σ and π ionic states included, we obtain an accuracy of about 10% for the $1\sigma_g$ channel. The single photon ionization to the shakeup channel $1\sigma_u$ is also computed to a few percent accuracy with 11 ionic states. We find that the single ionization continuum of H_2 is more complex unlike helium and it needs more than a single ionic state.

With 4 and 6 ionic states, we find artefacts on the two photon peaks. This is a result of a part of the quantum chemistry neutral that appears in the eigenvalue spectrum of the Hamiltonian as a spurious doubly excited state ($|s\rangle$). Let $|f_i\rangle$ be the eigenvectors of the N particle field free Hamiltonian to which $|\mathcal{G}\rangle$ contributes. We can find a state $|s\rangle$ such that

$$|s\rangle = |\mathcal{G}\rangle - \sum_i |f_i\rangle \langle f_i | \mathcal{G} \rangle \neq 0 \quad (43)$$

This spurious correlated state moves to higher with addition of ionic states. A straight forward solution to this problem is to compute this state and project it out of the basis. But, this would require locating the spurious state in the eigenvalue spectrum, which is very demanding for large Hamiltonians. Fortunately, by their dependence on the number of ionic states, artefacts of this kind are easily detected and can be moved out of the region of interest by using sufficiently many ionic states. This is a possible artefact one needs to be cautious about when dealing with wavefunction ansatz of kind (5).

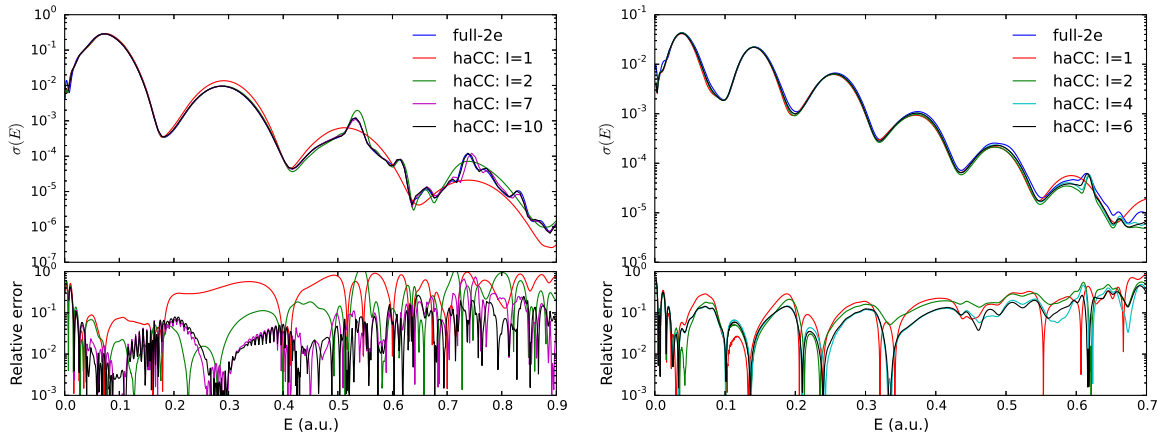


Figure 6. Total photoelectron spectra from H_2 with - Left figure: 3-cycle 200nm laser pulse with a peak intensity of $10^{14} W/cm^2$. Right figure: 3-cycle 400nm laser pulse with a peak intensity of $10^{14} W/cm^2$. The upper panels show spectra obtained with full-2e and haCC calculations with different number of ionic states (l) included as indicated in the legend. The lower panels show relative errors of haCC calculations with respect to the full-2e calculation.

Figure 6 shows total photoelectron spectra at 200nm and 400nm wavelengths. At 200nm, spectra are accurate up to 10% with 2 ionic states. Addition of more ionic states helps reproduce additional resonant features in the spectrum. Also at 400nm, 2 ionic states are sufficient to compute spectra that are accurate on 10% level, except for the resonant features. Inclusion of up to 6 ionic states reproduces the feature around 0.62 a.u. This feature in the 400nm spectrum may be identified with second or third $^1\Sigma_u^+$ doubly excited state [29].

We find that with H_2 at longer wavelengths, ground ionic state is sufficient to compute realistic spectra excluding the resonant features. Addition of more ionic states produces the additional features in the spectrum resulting from presence of correlated doubly excited states.

Figure 7 shows total ionization yield as a function of photon energy in the range 0.17-0.5 a.u. It shows a comparison of our haCC calculations with data available from other theoretical methods - time dependent CI method from [30] and FNA-TDSE (fixed nuclei approximation) method from [7]. The vertical lines in the figure separate different multi-photon ionization regimes. The general behavior of the yields from both CI and haCC procedure is the same. There is a discrepancy in the yields on the level of 15%. This may be a result of the intrinsic limitations of both the methods. There is a shift of about 0.2eV between the CI and haCC results around 0.3 a.u photon energy. The ionization potential of H_2 at equilibrium inter-nuclear distance ($R_0 = 1.4a.u$) is 0.604492 a.u (Table I in [31]). The ionization potential in our calculations is 0.6034 a.u, while it is around 0.59 a.u in time dependent CI calculations from [30] which can be read from the multi-photon thresholds presented there. Judging from the accuracy of the ionization thresholds, one may conclude that our haCC computations are more accurate than the CI results. The FNA-TDSE results from [7] have a similar qualitative behavior but are quantitatively quite different from our results and the CI results. The full-2e computations are expensive, especially at the ionization thresholds where large simulation box sizes are needed due to excitation of Rydberg states. Hence, we used this method to compute only at few points specially in the range where the FNA-TDSE and the haCC results have large discrepancies. We find that the full-2e calculations are consistent with the haCC results supporting the accuracy of our computations.

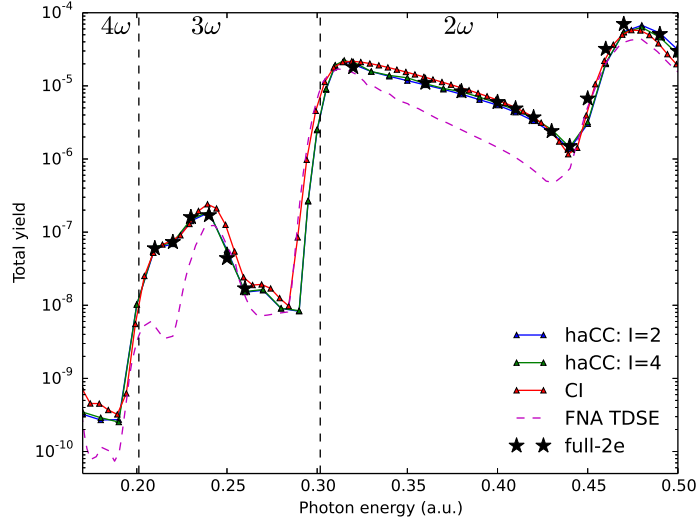


Figure 7. Ionization yield from H_2 at equilibrium internuclear distance ($R_0 = 1.4a.u.$) as a function of photon energy. Laser parameters: $10^{12}W/cm^2$ peak intensity, \cos^2 envelope pulses and 10fs pulse duration (In Eq (40) $2cT = 10fs$). A comparison of haCC calculations with 2,4 ionic states with CI results from [30] and FNA-TDSE results from [7]. The dashed vertical lines separate different multi-photon ionization regimes.

5. Conclusions

The hybrid anti-symmetrized Coupled Channels method introduced here opens the route to the reliable *ab initio* calculation of fully differential single photo-emission spectra from atoms and small molecules for a broad range of photon energies. It unites advanced techniques for the solution of the time-dependent Schrödinger equation for one- and two-electron systems in strong fields with state of the art quantum chemistry methods for the accurate description of electronic structure and field-induced bound state dynamics. For the specific implementation we have relied on a finite element implementation of the strong field dynamics and Gaussian-based CI package of COLUMBUS.

Key ingredients for the successful implementation are good performance of tSURFF for the computation of spectra from comparatively small spatial domains on the one hand and access to the well established technology of quantum chemistry on the other hand. We could obtain the quantum chemical structure in the form of the complete expansion into determinants from COLUMBUS. In future implementations, it may be sufficient to output from a given package the generalized one, two, and three-electron density matrices together with generalized Dyson orbitals, both defined in the present paper. It turned out to be instrumental for accurate results that haCC allows for the inclusion of neutral states in a natural fashion and at very low computational cost.

Several new techniques were introduced and implemented for the establishment of the method. Most notably, the mixed gauge approach [18] turned out to be crucial for being able to take advantage of the field-free electronic structure in presence of a strong field without abandoning the superior numerical properties of a velocity-gauge like calculation. The finite element method used for single-electron strong-field dynamics is convenient, but certainly not the only possible choice. Similar results should be achievable with higher order B-spline methods or any other discretization suitable for solutions of the single electron strong field Schrödinger equation. Low-rank updates are used in several places for the efficient computation of the inverses of the large overlap matrix and to control the linear dependency problems arising from anti-symmetrizing the essentially complete finite elements

basis against the Hartree-Fock orbitals.

We have made an effort to explore the potential range of applicability of the method by performing computations in a wide range of parameters on a few representative systems, where results can be checked against essentially complete methods. Spectra for the He atom were independently obtained from fully correlated two-electron calculations. We could demonstrate that haCC gives spectra on the accuracy level 10% with very low effort. An interesting observation is that in the long wavelength regime indeed a single ionization channel produces correct results, justifying *ex post* wide spread model approaches of the strong field community. As a note of caution, we recall that this is only possible as the *fully correlated initial state* is routinely included in the haCC scheme. At short wavelength, the ionic excited state dynamics plays a larger role and reliable results require inclusion of up to 9 ionic channels. With this we could correctly resolve also the peak due to He's doubly excited state.

The second atomic system, Be, was chosen to expose the role of ionic dynamics. While the $1s$ core electrons are energetically well-separated and no effect of their dynamics was discernable in a comparison with a frozen core model, the narrow spaced ionic states preclude single channel models. Depending on the observable and on desired accuracies, a minimum of two ionic channels had to be used.

For the comparison of H_2 photoionization and photoelectron spectra, we could refer to literature and supplemented the data with a full two-electron calculation. At 400nm, H_2 can be treated as a single channel system. At intermediate wavelengths, we find the need for at least two ionic channels, and we could obtain a fair agreement with comparison data. Here one has to take into consideration that all alternative methods operate near the limits of their applicability.

With this set of results we demonstrated the correctness of the method and its essential features. In our calculations, also the fundamental limitations of the approach were exposed. Clearly, the field-induced dynamics of the ionic part must be describable by a few states with bound character. haCC shares this limitation with any expansion that is limited to a few ionic states. Note that the problem is partly mitigated by the possibility to include fully correlated ground as well as singly- and doubly-excited states with bound-state character that are known to appear in the dynamics.

The method in its present implementation can be applied to small molecules such as N_2 and CO_2 which will be reported in a forthcoming publication. At the moment, the computation of the two-electron integrals poses a mild technical limitation for such calculations, and an improvement of the presently rather straight-forward algorithm is needed for going to larger systems. Another limitation arises when the molecule becomes too large for computing even strong field single-electron dynamics over its complete extension. At present, tSURFF allows us to limit computation boxes to the scale of $\sim 40 a.u.$. Also, for the single electron part, we use at present single-center expansions, which perform notoriously poorly if scattering centers are distributed over more than a few atomic units. This limitation may well be overcome by a more versatile single-electron discretization, though at significant implementation effort.

Other potential extensions are to double-emission. The tSURFF method was formulated for this situation. Combining such already sizable calculations with a dication described by quantum chemistry in the same spirit as here may be feasible. The formula presented can be readily extended to include that case. However, the scaling is poor such that one may only hope for the simple one- or two-channel situation to be feasible in practice. A cut-down version of such an approach can be used to include non-bound dynamics by describing a second electron's dynamics in a more flexible basis, however, without admitting its emission.

These lines of development will be pursued in forthcoming work.

Acknowledgements

The authors thank the COLUMBUS developers - Hans Lischka, University of Vienna; Thomas Müller, Forschungszentrum Jülich; Felix Plasser, University of Heidelberg and Jiri Pittner, J. Heyrovský Institute for their support with constructing the quantum chemistry interface. V.P.M. is a fellow of the EU Marie Curie ITN ‘CORINF’ and the International Max Planck Research School - Advanced Photon Science. A.Z acknowledges support from the DFG through excellence cluster ‘Munich Center for Advanced Photonics (MAP)’ and from the Austrian Science Foundation project ViCoM (F41).

Appendix A. Finite element basis

Let $\{r_0, r_1, \dots, r_n\}$ be points on the radial axis that define n intervals on the radial axis. In a finite element approach, the basis functions $f_i^n(r)$ are chosen such that

$$f_i^n(r) \begin{cases} \neq 0 & \text{if } r \in [r_{n-1}, r_n] \\ = 0 & \text{otherwise} \end{cases} \quad (\text{A.1})$$

The individual basis functions can be chosen from any complete space, for example, in our case we use scaled Legendre polynomials of typical orders 10-14. Here, we write the finite element index and the function index separately to emphasize that we have two convergence parameters: the order and the number of finite elements. The calculations converge quickly with increasing order compared to with increasing number of elements [32]. The basis functions should also be tailored to satisfy the continuity conditions. This may be accomplished through an orthogonalization procedure in each interval so that the functions on each interval satisfy the following conditions:

$$\begin{aligned} f_0^n(r_{n-1}) &= 1; & f_0^n(r_n) &= 0 \\ f_1^n(r_{n-1}) &= 0; & f_1^n(r_n) &= 1 \\ f_{i \neq 0,1}^n(r_{n-1}) &= 0; & f_{i \neq 0,1}^n(r_n) &= 0 \end{aligned} \quad (\text{A.2})$$

Even though we are solving a second order differential equation, it is sufficient to impose just the continuity condition to solve the differential equation. It can be shown through a simple computation, for example as shown in [32], that the matrix elements corresponding to the laplacian operator can be computed even if the functions are not differentiable at the finite element boundaries. This is because the δ -like terms arising due to the non-differentiability are compensated by the surface terms. The matrices corresponding to various operators in a finite element basis have a banded structure, that can be used to perform various linear algebra operations efficiently.

In a three-dimensional situation with spherical symmetry, these radial finite element functions can be multiplied by a complete set of angular basis functions such as the spherical harmonics to construct a three dimensional basis of the form $f_i^n(r)Y_{lm}(\theta, \phi)$.

References

- [1] M. Meckel, D. Comtois, D. Zeidler, A. Staudte, D. Pavii, H. C. Bandulet, H. Ppin, J. C. Kieffer, R. Drner, D. M. Villeneuve, and P. B. Corkum. Laser-induced electron tunneling and diffraction. *Science*, 320(5882):1478–1482, 2008.
- [2] R. Kienberger, E. Goulielmakis, M. Uiberacker, A. Baltuska, V. Yakovlev, F. Bammer, A. Scrinzi, Th. Westerwalbesloh, U. Kleineberg, U. Heinzmann, M. Drescher, and F. Krausz. Atomic transient recorder. *Nature*, 427(6977):817–821, February 2004.
- [3] Stefan Pabst and Robin Santra. Strong-field many-body physics and the giant enhancement in the high-harmonic spectrum of xenon. *Phys. Rev. Lett.*, 111:233005, Dec 2013.
- [4] Michael Spanner and Serguei Patchkovskii. One-electron ionization of multielectron systems in strong nonresonant laser fields. *Phys. Rev. A*, 80:063411, Dec 2009.

- [5] J. Jose, R. R. Lucchese, and T. N. Rescigno. Interchannel coupling effects in the valence photoionization of sf6. *The Journal of Chemical Physics*, 140(20):–, 2014.
- [6] J. M. Ngoko Djiokap and Anthony F. Starace. Resonant enhancement of the harmonic-generation spectrum of beryllium. *Phys. Rev. A*, 88:053412, Nov 2013.
- [7] A. Palacios, H. Bachau, and F. Martín. Enhancement and control of h2 dissociative ionization by femtosecond vuv laser pulses. *Phys. Rev. Lett.*, 96:143001, Apr 2006.
- [8] Henry Timmers, Zheng Li, Niranjana Shivaram, Robin Santra, Oriol Vendrell, and Arvinder Sandhu. Coherent electron hole dynamics near a conical intersection. *Phys. Rev. Lett.*, 113:113003, Sep 2014.
- [9] Loren Greenman, Phay J. Ho, Stefan Pabst, Eugene Kamarchik, David A. Mazziotti, and Robin Santra. Implementation of the time-dependent configuration-interaction singles method for atomic strong-field processes. *Phys. Rev. A*, 82:023406, Aug 2010.
- [10] J. Caillat, J. Zanghellini, M. Kitzler, O. Koch, W. Kreuzer, and A. Scrinzi. Correlated multielectron systems in strong laser fields: A multiconfiguration time-dependent hartree-fock approach. *Phys. Rev. A*, 71:012712, Jan 2005.
- [11] David Hochstuhl and Michael Bonitz. Time-dependent restricted-active-space configuration-interaction method for the photoionization of many-electron atoms. *Phys. Rev. A*, 86:053424, Nov 2012.
- [12] Haruhide Miyagi and Lars Bojer Madsen. Time-dependent restricted-active-space self-consistent-field theory for laser-driven many-electron dynamics. *Phys. Rev. A*, 87:062511, Jun 2013.
- [13] Takeshi Sato and Kenichi L. Ishikawa. Time-dependent complete-active-space self-consistent-field method for multielectron dynamics in intense laser fields. *Phys. Rev. A*, 88:023402, Aug 2013.
- [14] M. A. Lysaght, H. W. van der Hart, and P. G. Burke. Time-dependent r -matrix theory for ultrafast atomic processes. *Phys. Rev. A*, 79:053411, May 2009.
- [15] Liang Tao and Armin Scrinzi. Photo-electron momentum spectra from minimal volumes: the time-dependent surface flux method. *New Journal of Physics*, 14(1):013021–, 2012.
- [16] Armin Scrinzi. t -surff: fully differential two-electron photo-emission spectra. *New Journal of Physics*, 14(8):085008–, 2012.
- [17] Hans Lischka, Thomas Müller, Peter G. Szalay, Isaiah Shavitt, Russell M. Pitzer, and Ron Shepard. Columbus—a program system for advanced multireference theory calculations. *WIREs Comput Mol Sci*, 1(2):191–199, 2011.
- [18] Vinay Pramod Majety, Alejandro Zielinski, and Armin Scrinzi. Mixed gauge in strong laser-matter interaction. *arXiv:1408.6309*, Aug 2014.
- [19] Armin Scrinzi. Infinite-range exterior complex scaling as a perfect absorber in time-dependent problems. *Phys. Rev. A*, 81:053845, May 2010.
- [20] Alejandro Zielinski, Vinay Pramod Majety, and Armin Scrinzi. A general solver for the time-dependent schrödinger equation of one and two particle systems. (Unpublished).
- [21] M. Woodbury. Inverting modified matrices. *Memorandum Rept., 42, Statistical Research Group, Princeton University, Princeton, NJ*, 1950.
- [22] I. A. Ivanov and A. S. Kheifets. Strong-field ionization of he by elliptically polarized light in attoclock configuration. *Phys. Rev. A*, 89:021402, Feb 2014.
- [23] Petra Ruth Kaprálová-Žánská, Jan Šmydke, and Svatopluk Civiš. Excitation of helium rydberg states and doubly excited resonances in strong extreme ultraviolet fields: Full-dimensional quantum dynamics using exponentially tempered gaussian basis sets. *The Journal of Chemical Physics*, 139(10):–, 2013.
- [24] G. W. Drake. Theoretical energies for the $n=1$ and 2 states of the helium isoelectronic sequence up to $z=100$. *Canadian Journal of Physics*, 66(7):586–611, 1988.
- [25] Toru Morishita and C. D. Lin. Photoelectron spectra and high rydberg states of lithium generated by intense lasers in the over-the-barrier ionization regime. *Phys. Rev. A*, 87:063405, Jun 2013.
- [26] Keith Berrington, Lisa Quigley, and Hong Lin Zhang. The calculation of high-energy photoionization cross sections for the be isoelectronic sequence. *Journal of Physics B: Atomic, Molecular and Optical Physics*, 30(23):5409–, 1997.
- [27] R. Wehlitz, D. Lukić, and J. B. Bluett. Single and double photoionization of beryllium below 40 eV. *Phys. Rev. A*, 71:012707, Jan 2005.
- [28] Yulian V Vanne and Alejandro Saenz. Numerical treatment of diatomic two-electron molecules using a b-spline based ci method. *Journal of Physics B: Atomic, Molecular and Optical Physics*, 37(20):4101–, 2004.
- [29] I. Sánchez and F. Martín. The doubly excited states of the h2 molecule. *The Journal of Chemical Physics*, 106(18):7720–7730, 1997.
- [30] Johann Förster, Yulian V. Vanne, and Alejandro Saenz. Ionization behavior of molecular hydrogen in intense laser fields: Influence of molecular vibration and alignment. *Phys. Rev. A*, 90:053424, Nov 2014.
- [31] Armin Lühr, Yulian V. Vanne, and Alejandro Saenz. Parameter-free one-center model potential for an effective one-electron description of molecular hydrogen. *Phys. Rev. A*, 78:042510, Oct 2008.
- [32] Armin Scrinzi and Nils Elander. A finite element implementation of exterior complex scaling for the accurate determination of resonance energies. *The Journal of Chemical Physics*, 98(5):3866–3875, 1993.